

Article

Quantifying the Influence of a Burn Event on Ammonia Concentrations Using a Machine-Learning Technique

Jiabao Hu ^{1,2}, Tingting Liao ^{3,4,*}, Yixuan Lü ^{1,5}, Yanjun Wang ¹, Yuexin He ¹, Weishou Shen ², Xianyu Yang ^{3,4}, Dongsheng Ji ¹ and Yuepeng Pan ^{1,5,6,*} 

- ¹ State Key Laboratory of Atmospheric Boundary Layer Physics and Atmospheric Chemistry (LAPC), Institute of Atmospheric Physics, Chinese Academy of Sciences, Beijing 100029, China; hujiabao@nuist.edu.cn (J.H.); lvyixuan20@mailsucas.ac.cn (Y.L.); 201842859@mail.sdu.edu.cn (Y.W.); heyuexin15@mailsucas.ac.cn (Y.H.); jds@dq.cern.ac.cn (D.J.)
 - ² Collaborative Innovation Centre of Atmospheric Environment and Equipment Technology, Jiangsu Key Laboratory of Atmospheric Environment Monitoring and Pollution Control, School of Environmental Science and Engineering, Nanjing University of Information Science & Technology, Nanjing 210044, China; wsshshen@nuist.edu.cn
 - ³ The Plateau Atmosphere and Environment Key Laboratory of Sichuan Province, School of Atmospheric Science, Chengdu University of Information Technology, Chengdu 610225, China; xyang@cuit.edu.cn
 - ⁴ Chengdu Plain Urban Meteorology and Environment Observation and Research Station of Sichuan Province, Chengdu 610225, China
 - ⁵ College of Earth and Planetary Sciences, University of Chinese Academy of Sciences, Beijing 100049, China
 - ⁶ Artificial Intelligence Research Center for Atmospheric Science, Beijing 100029, China
- * Correspondence: ltt2014@cuit.edu.cn (T.L.); panyuepeng@mail.iap.ac.cn (Y.P.)



Citation: Hu, J.; Liao, T.; Lü, Y.; Wang, Y.; He, Y.; Shen, W.; Yang, X.; Ji, D.; Pan, Y. Quantifying the Influence of a Burn Event on Ammonia Concentrations Using a Machine-Learning Technique. *Atmosphere* **2022**, *13*, 170. <https://doi.org/10.3390/atmos13020170>

Academic Editors: Jacek Koziel, Xuejun Liu, Baojing Gu and Lin Zhang

Received: 19 November 2021

Accepted: 18 January 2022

Published: 21 January 2022

Publisher's Note: MDPI stays neutral with regard to jurisdictional claims in published maps and institutional affiliations.



Copyright: © 2022 by the authors. Licensee MDPI, Basel, Switzerland. This article is an open access article distributed under the terms and conditions of the Creative Commons Attribution (CC BY) license (<https://creativecommons.org/licenses/by/4.0/>).

Abstract: Although combustion is considered a common source of ammonia (NH₃) in the atmosphere, field measurements quantifying such emissions of NH₃ are still lacking. In this study, online measurements of NH₃ were performed by a cavity ring-down spectrometer, in the cold season at a rural site in Xianghe on the North China Plain. We found that the NH₃ concentrations were mostly below 65 ppb during the study period. However, from 18 to 21 November 2017, a close burn event (~100 m) increased the NH₃ concentrations to 145.6 ± 139.9 ppb. Using a machine-learning technique, we quantified that this burn event caused a significant increase in NH₃ concentrations by 411%, compared with the scenario without the burn event. In addition, the ratio of ΔNH₃/ΔCO during the burn period was 0.016, which fell in the range of biomass burning. Future investigations are needed to evaluate the impacts of the NH₃ combustion sources on air quality, ecosystems, and climate in the context of increasing burn events worldwide.

Keywords: random forest model; ammonia; burn events; combustion sources; China

1. Introduction

As an important alkaline gas in the atmosphere, atmospheric ammonia (NH₃) has a crucial influence on atmospheric chemistry and the nitrogen cycle [1,2]. It can react with sulfuric acid (H₂SO₄) and nitric acid (HNO₃), and enhance the formation of secondary inorganic aerosols (SIAs) [3]. Additionally, NH₃ can enhance the yield of secondary organic aerosols (SOAs) through aqueous chemistry [4]. These particulate SIAs and SOAs in the air decrease visibility, damage human health, and affect the climate [5–9]. After deposition, NH₃ can directly or indirectly affect terrestrial and aquatic ecosystems, such as soil acidification, water eutrophication, and reduction in biodiversity [10–12]. Thus, identifying and quantifying the sources of NH₃ is essential to understanding its vital role in atmospheric chemistry and reducing its negative impacts on the ecosystem and climate.

Although livestock waste and nitrogen fertilization are considered the most important sources of NH₃ emissions on a global or regional scale [13,14], NH₃ is also emitted into

the atmosphere during the fuel combustion process through pyrolysis [15]. Biomass burning, such as forest fires, plays a critical role in NH_3 emissions in rural areas. For example, 1.4–8.2 and 0.7–2.6 Tg of NH_3 were emitted from forest fires in Indonesia in autumn in 2015, and Russia in July–August 2010, respectively [16,17], and 0.12 Mt of NH_3 was emitted from agricultural crop residue burning in India from 2008 to 2009 [18]. In urban areas, the nitrogen isotopic approach indicates that NH_3 originated primarily from combustion sources, including coal combustion, NH_3 slip from power plants, and vehicle exhausts [19–21]. A high-resolution global inventory revealed that NH_3 emissions from combustion sources continued to increase from 1960 to 2013 [22]. In China, an average of 8182 forest fires occurred from 1987 to 2007 [23]. The elevated fire frequencies were partially due to climate change [24]. Thus, the impact of combustion sources on NH_3 concentrations and related consequences needs further attention.

China is a global hotspot of atmospheric NH_3 emissions, with an annual increasing rate of 1.9% [25]. Notably, the North China Plain (NCP) is confirmed to be the largest region with high surface concentrations, and the highest emissions in China [26]. Despite the pollution reduction actions implemented since 2013, severe haze pollution events still occur in the cold season in this region. For example, the highest $\text{PM}_{2.5}$ concentration reached approximately $250 \mu\text{g}/\text{m}^3$ in winter in 2020 [27], and it was dominated by sulfate–nitrate–ammonium (SNA), especially nitrate aerosols [28]. Recent studies have suggested that NH_3 plays an important role in determining nitrate concentrations [29,30]. Therefore, it is necessary to observe the concentrations of NH_3 and investigate its emission sources in this region.

In this study, we performed online measurements of NH_3 in the cold season in Xianghe, a rural site in NCP. During the observation campaign, we detected an unexpected burn event that had a significant influence on the NH_3 concentrations. Finally, we attempted to combine a novel machine-learning technique based on the random forest (RF) algorithm, to quantify the impact of burn events. Such an understanding could be beneficial for controlling NH_3 emissions and further improving air quality in the future.

2. Data and Methods

2.1. Site Description

Since 2017, online measurements of NH_3 concentrations have been performed in Xianghe, NCP (39.75°N , 116.96°E) (Figure 1). The site is surrounded by residential areas that lack tall buildings and obvious industrial emission sources. Based on its location in the northern part of the NCP between Beijing (~45 km) and Tianjin (~70 km), the instruments at the site can detect pollutants of urban, rural, background or mixed origins, reflecting the complex changes in NH_3 in the NCP.

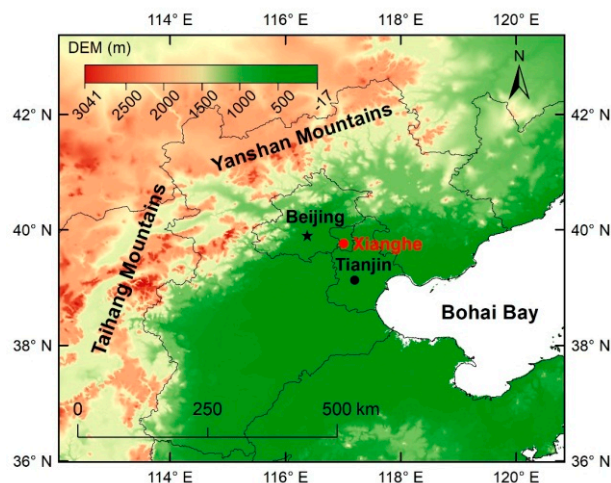


Figure 1. Location of the NH_3 observation site in Xianghe.

2.2. Data Sources

2.2.1. Measurements of NH₃

Hourly concentrations of NH₃ were measured at a high temporal resolution of 1 Hz, online, using a standard cavity ring-down spectrometer (CRDS) (G2103, Picarro Inc., Santa Clara, CA, USA). CRDS is a direct absorption technique that uses pulsed or continuous light sources and has a significantly higher sensitivity than conventional spectrometers [31]. In CRDS, two high reflectivity mirrors are used in the optical cavity to increase the absorption optical path length, thereby enhancing the contrast of the absorption signal of NH₃. The CRDS setting measures how long it takes for the light to drop to a certain percentage of its original intensity, and the “ring-down time” is used to calculate the concentration of NH₃ in the cavity [32].

To prevent water vapor from affecting the NH₃ spectrum, the manufacturer has incorporated a correction procedure for the reported NH₃ values [33]. In addition, to reduce the adsorption of NH₃, the Teflon tubing was insulated and warmed with heating tape (~45.7 °C). Meanwhile, a filter was installed at the front of the inlet to induce ambient air flow. According to the air conditions, the filter was replaced every 2 weeks to 1 month. The instrument was placed in an air-conditioned cabin laboratory; more detailed descriptions are documented elsewhere [34].

2.2.2. Other Supporting Data

Air pollutants and meteorological data are also used in this study. The hourly concentrations of SO₂, NO_x, CO, and PM_{2.5} were measured at the same height as NH₃. Meteorological parameters, including temperature (T), relative humidity (RH), wind speed (WS), and wind direction (WD), were obtained from the China Meteorological Administration (<http://data.cma.cn> (accessed on 14 October 2021)).

2.2.3. Burn Event

During the observation campaign, a burn event occurred from 18 to 21 November, 2017. This burn event was caused by the combustion of garbage in the nearby residential area, which was approximately 100 m away from the observation site. The burned material was complex and included discarded paper, kitchen waste, crop residues, weeds, branches, and leaves.

2.3. RF Models

The temporal variations in NH₃ in this study demonstrated a cycle ranging from 4 to 7 days. These strong cycles are regional in nature and controlled by the passage of cold fronts [35]. This unique temporal feature indicated that the results presented are reproducible on a regular basis, and applicable for the RF model in predicting NH₃ dynamics with meteorological conditions.

In this study, we used a machine-learning technique to quantify the influence of burn events on NH₃ concentrations. First, we established a model (RF1) with observed NH₃ concentrations as the dependent variable, and predictors (meteorological parameters, time predictors, and regional transport parameters) as the independent variables (Table 1). RF1 was trained on datasets during the nonburning period (8–17 and 22–30 November 2017). The training set accounted for 80% of data, and the testing set included the remaining 20%. On the basis of RF1, a series of models (RF2–RF11) were established, according to the relative importance of the predictor variables for eliminating or adding some predictors (Table S1). A detailed evaluation of all the established models is provided in Table S2, including the coefficients of determination (R²), the fraction of predictions within a factor of 2 (FAC2), mean bias, normalized mean bias, root-mean-square error (RMSE), and Pearson correlation coefficient (PCC). The performance of RF5 was considered the best due to its higher R² and lower RMSE.

The RF models were developed using the *rmweather* R package. However, unlike previous studies, we further adjusted two important parameters of RF5, namely, the number of trees (*ntree*) and the number of variables split in each node (*mtry*). *Mtry* values from 1 to

8 with an interval of 1, and ntree values from 50 to 500 with an interval of 50, were selected. As shown in Figure S1, when ntree was 300 and mtry was 5, the simulation effect of the model was best, as indicated by the higher R^2 value and lower prediction error (MSE).

Table 1. All possible predictors for the RF models in this study.

Codes	Prediction Variables	Units
Meteorological parameters		
T	Air Temperature	°C
WS	Wind speed	m/s
WD	Wind direction	degree
Pressure	Atmospheric pressure	hPa
RH	Relative humidity	%
Time parameters		
day_Julian	Date of the year (1–366)	n/a
weekday	Day of the week (1–7)	n/a
hour	Hour of the day (0–23)	n/a
Air pollutants		
PM _{2.5}	Particulate matter	µg/m ³
NO _x	Nitrogen oxides	µg/m ³
NO ₂	Nitrogen dioxide	µg/m ³
SO ₂	Sulfur dioxide	µg/m ³
CO	Carbon monoxide	ppb
NO	Nitrogen monoxide	µg/m ³
Regional transport parameter		
cluster	Back trajectory cluster	n/a

After the RF model was adjusted and optimized, the testing datasets were randomly selected to assess the correlation between the observed and predicted concentrations (Figure S2), to ensure that this model could make better predictions. Finally, we used this model to predict NH₃ concentrations under the assumption of no burn events. To evaluate the impact of the burn events (18–21 November 2017) on NH₃ concentrations, relative changes (R) between the observed concentrations ($C_{observed}$) and predicted concentrations ($C_{predicted}$) for NH₃ were defined using the following equation:

$$R = \frac{C_{observed} - C_{predicted}}{C_{predicted}} \times 100\% \quad (1)$$

3. Results and Discussion

3.1. Changes in Observed Concentrations of NH₃

Hourly concentrations of NH₃ were selected from 8 to 30 November 2017 in this study, and their temporal variations are shown in Figure 2. We found that the NH₃ concentrations were mostly below 65 ppb during the study period, with the exception of 18–21 November, when a burn event occurred. Therefore, in the following sections, we have separated the dataset into two periods, i.e., the burning period (18–21 November 2017) and the nonburning period (8–17 and 22–30 November 2017).

During the nonburning period, the NH₃ concentrations in Xianghe ranged from 1.9 to 154.3 ppb, with a mean value of 25.4 ± 16.9 ppb. The NH₃ concentrations in this study were comparable to the urban observations (28.5 ± 11.6 ppb) in autumn in Beijing [36]. Moreover, the average NH₃ level measured in Xianghe was generally similar to observations in India (24.6 ± 5.0 ppb) [37], but much higher than those in Europe (1.2 ppb) and the United States (2.4 ppb) in autumn [10,38].

After the start of the burn event, the observed concentrations of NH₃ significantly increased, with the highest value exceeding 600 ppb. In addition, three concentration spikes

occurred: at 7:00, 18 November (281.6 ppb); 2:00, 19 November (547.1 ppb); and 10:00, 20 November (601.4 ppb). During the burning period, the average NH_3 concentration was 145.6 ± 139.9 ppb, which is five times that in a previous report (26.6 ± 13.9 ppb) at the Xianghe site in the cold season [39].

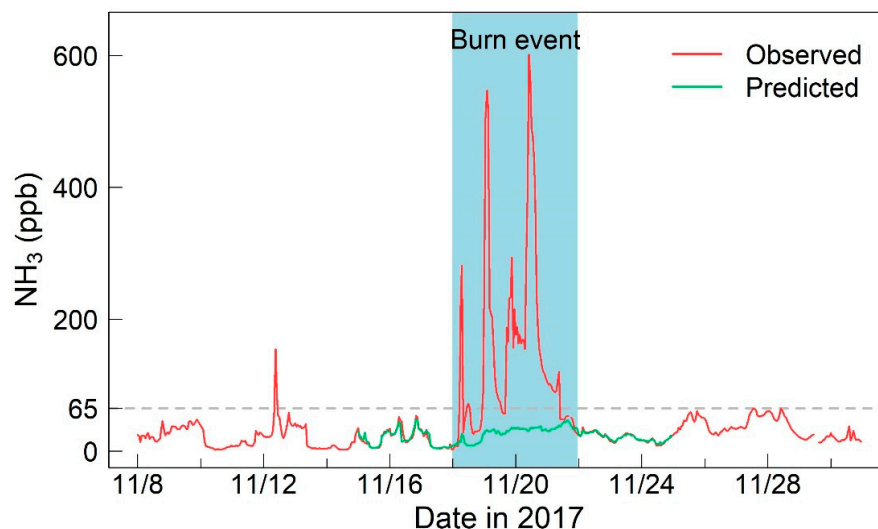


Figure 2. Temporal variation in hourly concentrations of NH_3 . The gray line indicates an NH_3 concentration of 65 ppb. The blue shaded area represents the burning period, and the non-shaded area represents the nonburning period.

In addition to NH_3 , the concentrations of other air pollutants also significantly increased during the burning period, e.g., by 209.7%, 84.3%, 69.1%, and 79.8% for $\text{PM}_{2.5}$, SO_2 , NO_x , and CO, respectively (Figure S3). These air pollutants had a positive correlation with NH_3 during the burning period, especially CO ($R^2 = 0.74$, $p < 0.01$) and NO_x ($R^2 = 0.72$, $p < 0.01$). However, their positive correlation was not significant in the nonburning period (Table S3). These results all indicated the potential influence of combustion sources on air quality. In addition, the intensity of combustion was closely related to weather conditions [40]. In our study, the NH_3 concentrations were higher during the burning period when the air mass originated from the northwest, and had a higher RH ($56.2 \pm 26.3\%$) and lower T (-1.1 ± 5 °C) and WS (1.6 ± 1.5 m s^{-1}) (Figure S4). To quantify the impact of the burn events on NH_3 , we predicted NH_3 concentrations without burn events using a machine-learning technique in the next section.

3.2. Changes in Predicted Concentrations of NH_3

We first established a model (RF5) to predict the NH_3 concentrations assuming that no burn event occurred from 18 to 21 November 2017. The predicted results are shown in Figure 2, with all predicted concentrations lower than 65 ppb. In addition, the temporal variation in predicted NH_3 concentrations was basically similar to its observed value in the nonburning period. This finding indicates that the concentrations and temporal pattern of NH_3 will not change significantly if there is no burn event.

The difference between the predicted and observed concentrations of NH_3 allows us to quantify the impacts of burn events on NH_3 emissions. As shown in Figure 3 and Table S4, remarkable differences were not found between the observed and predicted concentrations of NH_3 before the burn event, indicating that our model captured the variations in NH_3 concentrations well. However, the observed concentration of NH_3 increased drastically compared with the predicted value during the burning period, with increased ratios of 336.9%, 561.1%, and 652.2% in the first three days of the burn event. At the end of the burning period and with the resumption of “normal emissions”, the predicted values were consistent with the observations after 22 November. Overall, the observed and predicted concentrations of NH_3 during the burning period were 145.6 ± 139.9 and 28.5 ± 10.4 ppb,

respectively, resulting in an increase of 411%. These results indicated that the combustion source is an important factor of NH₃ emissions.

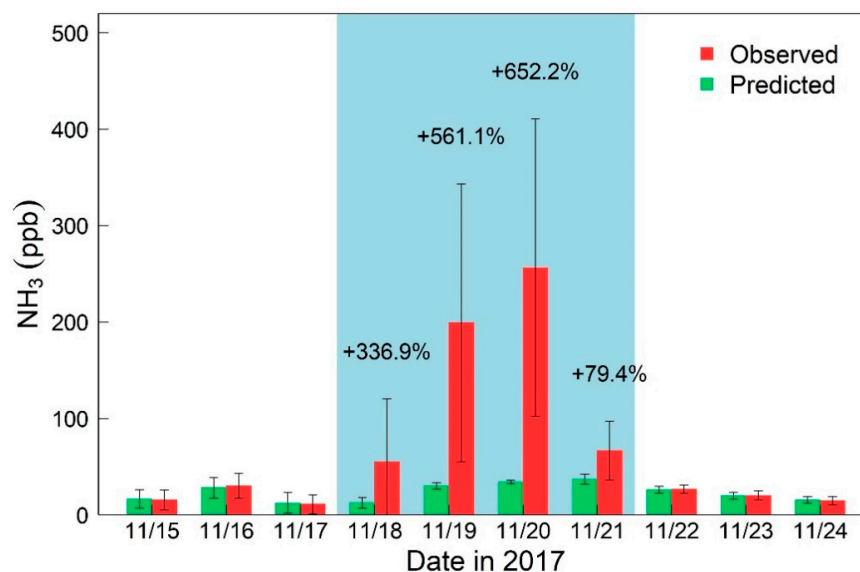


Figure 3. Observed and predicted concentrations of NH₃ before, during and after the burning period at the Xianghe site. Percentages on bars indicate relative changes (R) between the observed and predicted concentrations.

3.3. Dominant Source of NH₃ during the Burn Event

Although the overall impacts of the burn event on NH₃ concentrations were identified in the above sections, the potential dominant source contributing to the substantial increase in NH₃ was still unclear. To address this concern, we further investigated the relationship between NH₃ and other air pollutants.

As shown in Figure 4, we found that the ratio of NH₃ to other air pollutants significantly increased after the burn event occurred. Compared with those before burn events, the ratio of NH₃/PM_{2.5}, NH₃/SO₂, NH₃/NO_x, and NH₃/CO increased by a factor of 1.6, 2.5, 3.0, and 5.4 during the burning period, respectively (Table S5). This finding indicated a dramatic change of CO during the burn event. Thus, CO was selected as a tracer of fire [41]. Then, the emission ratio (ER) was defined as ΔNH₃/ΔCO in our study [17,42], where ΔNH₃ and ΔCO represented the difference in the corresponding concentrations of NH₃ and CO before and during the burn event. In this study, the calculated ΔNH₃/ΔCO value was 0.016, which was consistent with the characteristics of biomass burning (Table 2). Therefore, the dominant source emitting substantial NH₃ might be biomass burning in this burn event. Future control measures on NH₃ emissions should pay more attention to potential contributions from biomass burning.

Table 2. Summary of the NH₃ concentration and its emission ratio (ER = ΔNH₃/ΔCO) in different burn events.

Focus Region	Event	NH ₃ (ppb)		ER (ppb/ppb)	Reference
		Range	Average		
Xianghe, China	Biomass burning	2.4–601.4	145.6 ± 139.9	0.016	this study
Shenyang, China	Vehicular exhaust	61.8–248.3	152.9 ± 55.6	–	[43]
Canada and U.S.	Forest fire	7–130	–	0.012	[44]
Yucatan, Mexico	Biomass burning	–	–	0.022	[45]
California, U.S.	Biomass burning	–	–	0.019	[46]
Colorado, U.S.	Wildfires	<150	–	0.027	[47]
the Flint Hills, U.S.	Grassland fire	–	95	–	[48]
Western U.S.	Wildfires	>400	–	–	[49]

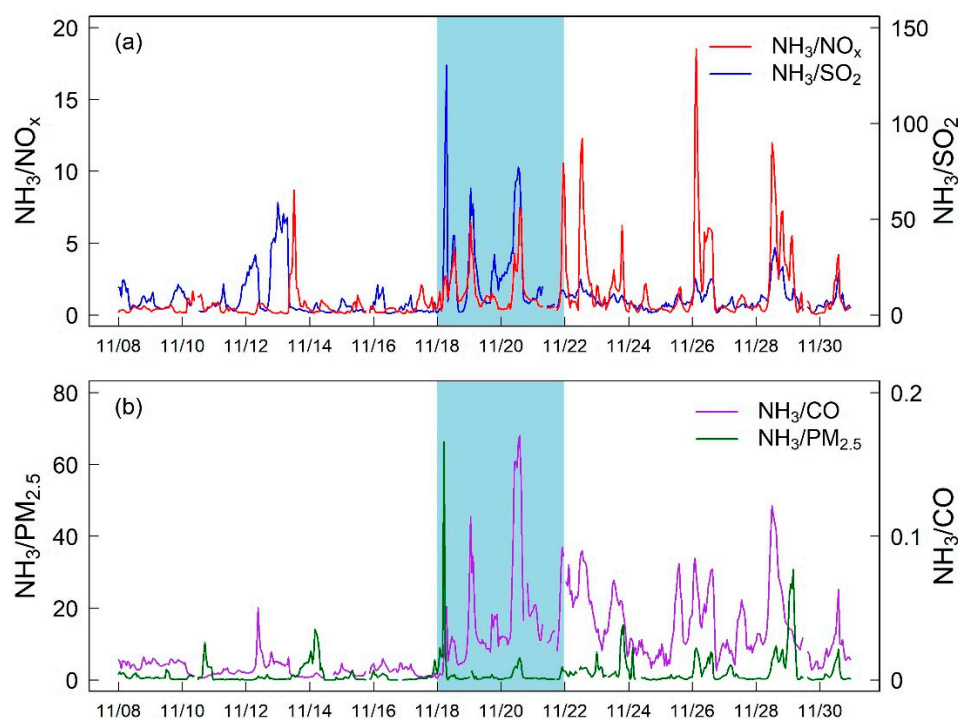


Figure 4. Temporal variation in the ratio of NH₃ relative to NO_x, SO₂ (a), CO and PM_{2.5} (b).

4. Conclusions

In this study, the NH₃ concentrations were measured by the CRDS technique in the cold season at a rural site in the NCP. The hourly NH₃ concentrations were mostly below 65 ppb during the study period. However, an unexpected burn event caused a significant increase in NH₃ concentration from 18 to 21 November 2017, with peak values exceeding 600 ppb. With the aid of a machine-learning technique, we found that the burn event could cause a 411% increase in the NH₃ concentration. Notably, the $\Delta\text{NH}_3/\Delta\text{CO}$ ratio was 0.016 during the burning period, indicating that biomass burning might be the dominant emission source. Due to the increasing occurrence of burn events worldwide, the impacts of the combustion sources of NH₃ on air quality, ecosystems, and climate need to be further explored.

Supplementary Materials: The following are available online at <https://www.mdpi.com/article/10.3390/atmos13020170/s1>: Figure S1: Influence of different ntree and mtry values on RF model; Figure S2: Performance of the RF model in predicting the NH₃ concentrations; Figure S3: Temporal variation of hourly concentrations of PM_{2.5}, SO₂, NO_x, and CO; Figure S4: Hourly variation of meteorological parameters; Table S1: Summary of 11 RF models and their predictors in this study; Table S2: Model validation in 11 RF models in this study; Table S3: Correlation matrix of NH₃, other air pollutants and meteorological parameters during the burning period; Table S4: Observed and predicted concentrations of NH₃ at the Xianghe site during the burning period; Table S5: Range and average of the ratio between NH₃ and other air pollutants before and during the burn event.

Author Contributions: Conceptualization, Y.P.; methodology, J.H.; software, J.H., Y.W. and Y.H.; validation, J.H.; formal analysis, J.H.; investigation, J.H. and Y.L.; resources, Y.P., D.J. and T.L.; data curation, J.H.; writing—original draft preparation, J.H.; writing—review and editing, Y.P. and W.S.; visualization, J.H.; supervision, Y.P. and W.S.; project administration, Y.P. and X.Y.; funding acquisition, Y.P., T.L. and X.Y. All authors have read and agreed to the published version of the manuscript.

Funding: This research was funded by the National Natural Science Foundation of China [grant number 42077204] and the Open Research Fund Program of Plateau Atmosphere and Environment Key Laboratory of Sichuan Province (Project PAEKL-2020-C3).

Institutional Review Board Statement: Not applicable.

Informed Consent Statement: Not applicable.

Data Availability Statement: The data presented in this study are available on reasonable request from the corresponding author.

Conflicts of Interest: The authors declare no conflict of interest.

References

1. Zhao, Y.; Zhang, L.; Pan, Y.; Wang, Y.; Paulot, F.; Henze, D.K. Atmospheric nitrogen deposition to the northwestern Pacific: Seasonal variation and source attribution. *Atmos. Chem. Phys.* **2015**, *15*, 10905–10924. [[CrossRef](#)]
2. Wen, Z.; Xu, W.; Li, Q.; Han, M.; Tang, A.; Zhang, Y.; Luo, X.; Shen, J.; Wang, W.; Li, K.; et al. Changes of nitrogen deposition in China from 1980 to 2018. *Environ. Int.* **2020**, *144*, 106022. [[CrossRef](#)] [[PubMed](#)]
3. Pan, Y.; Tian, S.; Liu, D.; Fang, Y.; Zhu, X.; Zhang, Q.; Zheng, B.; Michalski, G.; Wang, Y. Fossil fuel combustion-related emissions dominate atmospheric ammonia sources during severe haze episodes: Evidence from ¹⁵N-stable isotope in size-resolved aerosol ammonium. *Environ. Sci. Technol.* **2016**, *50*, 8049–8056. [[CrossRef](#)]
4. Fu, X.; Wang, S.; Xing, J.; Zhang, X.; Wang, T.; Hao, J. Increasing ammonia concentrations reduce the effectiveness of particle pollution control achieved via SO₂ and NO_x emissions reduction in east China. *Environ. Sci. Technol. Lett.* **2017**, *4*, 221–227. [[CrossRef](#)]
5. Chen, W.; Tong, D.Q.; Dan, M.; Zhang, S.; Zhang, X.; Pan, Y. Typical atmospheric haze during crop harvest season in northeastern China: A case in the Changchun region. *J. Environ. Sci.* **2017**, *54*, 101–113. [[CrossRef](#)] [[PubMed](#)]
6. Xin, J.; Wang, Y.; Wang, L.; Tang, G.; Sun, Y.; Pan, Y.; Ji, D. Reductions of PM_{2.5} in Beijing-Tianjin-Hebei urban agglomerations during the 2008 Olympic Games. *Adv. Atmos. Sci.* **2012**, *29*, 1330–1342. [[CrossRef](#)]
7. Li, W.; Liu, X.; Zhang, Y.; Sun, K.; Wu, Y.; Xue, R.; Zeng, L.; Qu, Y.; An, J. Characteristics and formation mechanism of regional haze episodes in the Pearl River Delta of China. *J. Environ. Sci.* **2018**, *63*, 236–249. [[CrossRef](#)]
8. Wu, J.; Wu, Y.; Tian, Y.; Wu, Y.; Wang, M.; Wang, X.; Wang, Z.; Hu, Y. Association between ambient fine particulate matter and adult hospital admissions for pneumonia in Beijing, China. *Atmos. Environ.* **2020**, *231*, 117497. [[CrossRef](#)]
9. Zhu, L.; Henze, D.K.; Bash, J.O.; Cady-Pereira, K.E.; Shephard, M.W.; Luo, M.; Capps, S.L. Sources and impacts of atmospheric NH₃: Current understanding and frontiers for modeling, measurements, and remote sensing in North America. *Curr. Pollut. Rep.* **2015**, *1*, 95–116. [[CrossRef](#)]
10. Felix, J.D.; Elliott, E.M.; Gay, D.A. Spatial and temporal patterns of nitrogen isotopic composition of ammonia at U.S. ammonia monitoring network sites. *Atmos. Environ.* **2017**, *150*, 434–442. [[CrossRef](#)]
11. Liu, M.; Huang, X.; Song, Y.; Tang, J.; Cao, J.; Zhang, X.; Zhang, Q.; Wang, S.; Xu, T.; Kang, L.; et al. Ammonia emission control in China would mitigate haze pollution and nitrogen deposition, but worsen acid rain. *Proc. Natl. Acad. Sci. USA* **2019**, *116*, 7760. [[CrossRef](#)] [[PubMed](#)]
12. Pan, Y.; Gu, M.; He, Y.; Wu, D.; Liu, C.; Song, L.; Tian, S.; Lü, X.; Sun, Y.; Song, T.; et al. Revisiting the concentration observations and source apportionment of atmospheric ammonia. *Adv. Atmos. Sci.* **2020**, *37*, 933–938. [[CrossRef](#)]
13. Kong, L.; Tang, X.; Zhu, J.; Wang, Z.; Pan, Y.; Wu, H.; Wu, L.; Wu, Q.; He, Y.; Tian, S.; et al. Improved inversion of monthly ammonia emissions in China based on the Chinese ammonia monitoring network and ensemble kalman filter. *Environ. Sci. Technol.* **2019**, *53*, 12529–12538. [[CrossRef](#)] [[PubMed](#)]
14. Kang, Y.; Liu, M.; Song, Y.; Huang, X.; Yao, H.; Cai, X.; Zhang, H.; Kang, L.; Liu, X.; Yan, X.; et al. High-resolution ammonia emissions inventories in China from 1980 to 2012. *Atmos. Chem. Phys.* **2016**, *16*, 2043–2058. [[CrossRef](#)]
15. Ozgen, S.; Cernuschi, S.; Caserini, S. An overview of nitrogen oxides emissions from biomass combustion for domestic heat production. *Renew. Sustain. Energy Rev.* **2021**, *135*, 110113. [[CrossRef](#)]
16. Whitburn, S.; Van Damme, M.; Clarisse, L.; Turquety, S.; Clerbaux, C.; Coheur, P.-F. Doubling of annual ammonia emissions from the peat fires in Indonesia during the 2015 El Niño. *Geophys. Res. Lett.* **2016**, *43*, 11007–11014. [[CrossRef](#)]
17. R'Honi, Y.; Clarisse, L.; Clerbaux, C.; Hurtmans, D.; Dufлот, V.; Turquety, S.; Ngadi, Y.; Coheur, P.F. Exceptional emissions of NH₃ and HCOOH in the 2010 Russian wildfires. *Atmos. Chem. Phys.* **2013**, *13*, 4171–4181. [[CrossRef](#)]
18. Jain, N.; Bhatia, A.; Pathak, H. Emission of air pollutants from crop residue burning in India. *Aerosol Air Qual. Res.* **2014**, *14*, 422–430. [[CrossRef](#)]
19. Pan, Y.; Tian, S.; Liu, D.; Fang, Y.; Zhu, X.; Gao, M.; Gao, J.; Michalski, G.; Wang, Y. Isotopic evidence for enhanced fossil fuel sources of aerosol ammonium in the urban atmosphere. *Environ. Pollut.* **2018**, *238*, 942–947. [[CrossRef](#)]
20. Pan, Y.; Tian, S.; Liu, D.; Fang, Y.; Zhu, X.; Gao, M.; Wentworth, G.R.; Michalski, G.; Huang, X.; Wang, Y. Source apportionment of aerosol ammonium in an ammonia-rich atmosphere: An isotopic study of summer clean and hazy days in urban Beijing. *J. Geophys. Res.* **2018**, *123*, 5681–5689. [[CrossRef](#)]
21. Gu, M.; Pan, Y.; Walters, W.W.; Sun, Q.; Song, L.; Wang, Y.; Xue, Y.; Fang, Y. Vehicular emissions enhanced ammonia concentrations in winter mornings: Insights from diurnal nitrogen isotopic signatures. *Environ. Sci. Technol.* **2022**. [[CrossRef](#)]
22. Meng, W.; Zhong, Q.; Yun, X.; Zhu, X.; Huang, T.; Shen, H.; Chen, Y.; Chen, H.; Zhou, F.; Liu, J.; et al. Improvement of a global high-resolution ammonia emission inventory for combustion and industrial sources with mew data from the residential and transportation sectors. *Environ. Sci. Technol.* **2017**, *51*, 2821–2829. [[CrossRef](#)] [[PubMed](#)]

23. Chang, Y.; Zhu, Z.; Bu, R.; Li, Y.; Hu, Y. Environmental controls on the characteristics of mean number of forest fires and mean forest area burned (1987–2007) in China. *For. Ecol. Manag.* **2015**, *356*, 13–21. [[CrossRef](#)]
24. Xiong, Q.; Luo, X.; Liang, P.; Xiao, Y.; Xiao, Q.; Sun, H.; Pan, K.; Wang, L.; Li, L.; Pang, X. Fire from policy, human interventions, or biophysical factors? Temporal–spatial patterns of forest fire in southwestern China. *For. Ecol. Manag.* **2020**, *474*, 118381. [[CrossRef](#)]
25. Zhang, X.; Wu, Y.; Liu, X.; Reis, S.; Jin, J.; Dragosits, U.; Van Damme, M.; Clarisse, L.; Whitburn, S.; Coheur, P.-F.; et al. Ammonia emissions may be substantially underestimated in China. *Environ. Sci. Technol.* **2017**, *51*, 12089–12096. [[CrossRef](#)]
26. Pan, Y.; Tian, S.; Zhao, Y.; Zhang, L.; Zhu, X.; Gao, J.; Huang, W.; Zhou, Y.; Song, Y.; Zhang, Q.; et al. Identifying ammonia hotspots in China using a national observation network. *Environ. Sci. Technol.* **2018**, *52*, 3926–3934. [[CrossRef](#)]
27. Sun, Y.; Lei, L.; Zhou, W.; Chen, C.; He, Y.; Sun, J.; Li, Z.; Xu, W.; Wang, Q.; Ji, D.; et al. A chemical cocktail during the COVID-19 outbreak in Beijing, China: Insights from six-year aerosol particle composition measurements during the Chinese New Year holiday. *Sci. Total Environ.* **2020**, *742*, 140739. [[CrossRef](#)] [[PubMed](#)]
28. Li, J.; Wu, Y.; Ren, L.; Wang, W.; Tao, J.; Gao, Y.; Li, G.; Yang, X.; Han, Z.; Zhang, R. Variation in PM_{2.5} sources in central North China Plain during 2017–2019: Response to mitigation strategies. *J. Environ. Manag.* **2021**, *288*, 112370. [[CrossRef](#)]
29. Wang, Y.; Zhang, Q.Q.; He, K.; Zhang, Q.; Chai, L. Sulfate-nitrate-ammonium aerosols over China: Response to 2000–2015 emission changes of sulfur dioxide, nitrogen oxides, and ammonia. *Atmos. Chem. Phys.* **2013**, *13*, 2635–2652. [[CrossRef](#)]
30. Xu, Z.; Liu, M.; Zhang, M.; Song, Y.; Wang, S.; Zhang, L.; Xu, T.; Wang, T.; Yan, C.; Zhou, T.; et al. High efficiency of livestock ammonia emission controls in alleviating particulate nitrate during a severe winter haze episode in northern China. *Atmos. Chem. Phys.* **2019**, *19*, 5605–5613. [[CrossRef](#)]
31. Berden, G.; Peeters, R.; Meijer, G. Cavity ring-down spectroscopy: Experimental schemes and applications. *Int. Rev. Phys. Chem.* **2000**, *19*, 565–607. [[CrossRef](#)]
32. von Bobruzki, K.; Braban, C.F.; Famulari, D.; Jones, S.K.; Blackall, T.; Smith, T.E.L.; Blom, M.; Coe, H.; Gallagher, M.; Ghalaieny, M.; et al. Field inter-comparison of eleven atmospheric ammonia measurement techniques. *Atmos. Meas. Tech.* **2010**, *3*, 91–112. [[CrossRef](#)]
33. Martin, N.A.; Ferracci, V.; Cassidy, N.; Hoffnagle, J.A. The application of a cavity ring-down spectrometer to measurements of ambient ammonia using traceable primary standard gas mixtures. *Appl. Phys. B* **2016**, *122*, 219. [[CrossRef](#)]
34. He, Y.; Pan, Y.; Zhang, G.; Ji, D.; Tian, S.; Xu, X.; Zhang, R.; Wang, Y. Tracking ammonia morning peak, sources and transport with 1 Hz measurements at a rural site in North China Plain. *Atmos. Environ.* **2020**, *235*, 117630. [[CrossRef](#)]
35. Jia, Y.; Rahn, K.A.; He, K.; Wen, T.; Wang, Y. A novel technique for quantifying the regional component of urban aerosol solely from its sawtooth cycles. *J. Geophys. Res.* **2008**, *113*, D21309. [[CrossRef](#)]
36. Pu, W.; Ma, Z.; Collett, J.L., Jr.; Guo, H.; Lin, W.; Cheng, Y.; Quan, W.; Li, Y.; Dong, F.; He, D. Regional transport and urban emissions are important ammonia contributors in Beijing, China. *Environ. Pollut.* **2020**, *265*, 115062. [[CrossRef](#)] [[PubMed](#)]
37. Saraswati; Sharma, S.K.; Mandal, T.K. Five-year measurements of ambient ammonia and its relationships with other trace gases at an urban site of Delhi, India. *Meteorol. Atmos. Phys.* **2018**, *130*, 241–257. [[CrossRef](#)]
38. Backes, A.; Aulinger, A.; Bieser, J.; Matthias, V.; Quante, M. Ammonia emissions in Europe, part I: Development of a dynamical ammonia emission inventory. *Atmos. Environ.* **2016**, *131*, 55–66. [[CrossRef](#)]
39. He, Y.; Pan, Y.; Gu, M.; Sun, Q.; Zhang, Q.; Zhang, R.; Wang, Y. Changes of ammonia concentrations in wintertime on the North China Plain from 2018 to 2020. *Atmos. Res.* **2021**, *253*, 105490. [[CrossRef](#)]
40. Li, Y.; Liu, J.; Han, H.; Zhao, T.; Zhang, X.; Zhuang, B.; Wang, T.; Chen, H.; Wu, Y.; Li, M. Collective impacts of biomass burning and synoptic weather on surface PM_{2.5} and CO in Northeast China. *Atmos. Environ.* **2019**, *213*, 64–80. [[CrossRef](#)]
41. Whitburn, S.; Van Damme, M.; Clarisse, L.; Hurtmans, D.; Clerbaux, C.; Coheur, P.F. IASI-derived NH₃ enhancement ratios relative to CO for the tropical biomass burning regions. *Atmos. Chem. Phys.* **2017**, *17*, 12239–12252. [[CrossRef](#)]
42. Andreae, M.O.; Merlet, P. Emission of trace gases and aerosols from biomass burning. *Glob. Biogeochem. Cycles* **2001**, *15*, 955–966. [[CrossRef](#)]
43. Song, L.; Walters, W.W.; Pan, Y.; Li, Z.; Gu, M.; Duan, Y.; Lü, X.; Fang, Y. ¹⁵N natural abundance of vehicular exhaust ammonia, quantified by active sampling techniques. *Atmos. Environ.* **2021**, *255*, 118430. [[CrossRef](#)]
44. Hegg, D.A.; Radke, L.F.; Hobbs, P.V.; Riggan, P.J. Ammonia emissions from biomass burning. *Geophys. Res. Lett.* **1988**, *15*, 335–337. [[CrossRef](#)]
45. Yokelson, R.J.; Crouse, J.D.; DeCarlo, P.F.; Karl, T.; Urbanski, S.; Atlas, E.; Campos, T.; Shinozuka, Y.; Kapustin, V.; Clarke, A.D.; et al. Emissions from biomass burning in the Yucatan. *Atmos. Chem. Phys.* **2009**, *9*, 5785–5812. [[CrossRef](#)]
46. Akagi, S.K.; Craven, J.S.; Taylor, J.W.; McMeeking, G.R.; Yokelson, R.J.; Burling, I.R.; Urbanski, S.P.; Wold, C.E.; Seinfeld, J.H.; Coe, H.; et al. Evolution of trace gases and particles emitted by a chaparral fire in California. *Atmos. Chem. Phys.* **2012**, *12*, 1397–1421. [[CrossRef](#)]
47. Benedict, K.B.; Prenni, A.J.; Carrico, C.M.; Sullivan, A.P.; Schichtel, B.A.; Collett, J.L. Enhanced concentrations of reactive nitrogen species in wildfire smoke. *Atmos. Environ.* **2017**, *148*, 8–15. [[CrossRef](#)]
48. Baker, K.; Koplitz, S.; Foley, K.; Avey, L.; Hawkins, A. Characterizing grassland fire activity in the Flint Hills region and air quality using satellite and routine surface monitor data. *Sci. Total Environ.* **2019**, *659*, 1555–1566. [[CrossRef](#)] [[PubMed](#)]
49. Lindaas, J.; Pollack, I.B.; Calahorrano, J.J.; O'Dell, K.; Garofalo, L.A.; Pothier, M.A.; Farmer, D.K.; Kreidenweis, S.M.; Campos, T.; Flocke, F.; et al. Empirical insights into the fate of ammonia in western U.S. Wildfire smoke plumes. *J. Geophys. Res.* **2021**, *126*, e2020JD033730. [[CrossRef](#)]